MONITORING THE DISBONDING OF A CFRP PLATE-BONDED REINFORCEMENT OF A STRUCTURAL BEAM USING A CHIRPED FBG SENSOR

A.R.Sanderson[1]*, S.L.Ogin[1], T.F.Capell[1], A.D.Crocombe[1], M.R.L Gower[2], E.Barton[2], R.J.Lee[3], J.Hawker[4].

[1]*Faculty of Engineering and Physical Sciences, University of Surrey, Guildford, United Kingdom.*
[2]*National Physical Laboratory, Teddington, United Kingdom.*
[3]*ESR Technology Ltd, Abingdon, United Kingdom.*
[4]*Marine and Technology Division, Babcock International Group, Devonport Royal Dockyard, Plymouth, United Kingdom.*
**A.R.Sanderson@surrey.ac.uk*

Keywords: Chirped fibre Bragg grating (CFBG); Structural health monitoring (SHM); Disbonding.

Abstract

A surface-mounted CFBG sensor has been used to monitor disbond growth of a CFRP plate-bonded reinforcement of a structural box-section beam, bonded using a room-temperature cure structural adhesive. These tests are part of a programme to determine whether disbonding of such a plate could be monitored by ambient thermal fluctuations alone with the aid of thermal mismatch strains. Disbonds were introduced by physically cutting the structural adhesive and a range of different disbond lengths and temperatures have been investigated. When monitoring the disbond growth using the CFBG sensors, a distinct peak-trough perturbation in the reflected spectra was indicative of the location of the disbond front during the test. A prediction of the reflected spectrum was in good agreement with the experimentally-determined results, enabling the disbond lengths to be measured using the CFBG sensor technique to within about 3 mm.

1 Introduction

The use of composite reinforcement of civil structures, such as bridges, is becoming increasingly prevalent in civil sectors, with so much of the country's ageing civil infrastructure difficult to cost-effectively replace. Composite reinforcement of existing structures has many benefits, such as arresting existing non-critical damage, and increasing the operational lifetime of a structure, all at a reasonable cost when compared to replacing the structure. However, the introduction of a plate-bonded reinforcement introduces new potential failure modes, such as the disbonding of the reinforcement from the structure as a consequence of defects in the initial bondline, impact or other damage to the plate, or environmental degradation of the bondline. The ability to detect disbond initiation and/or growth would be very useful for assessing the structure's continued viability. Various NDE (non-destructive evaluation) techniques are potentially able to detect the location of such disbonds, including acoustic emission, electric resistance measurements, shearography and thermography [e.g.1-3]. It is, though, likely to be difficult to employ many of the currently proposed techniques either due to the unproven nature of the technique or the physical

difficulties of implementation (e.g. complications arising out of the connections required). Regarding fibre optic sensors, the ability to be able to embed such sensors within a composite structure, and the proven usage of fibre optical sensors for monitoring large structures [e.g. 4] make these sensors important candidates.

The use of CFBG optical sensors for monitoring damage development (e.g. disbonding in lap joints; mode I crack growth in DCB specimens) has been described elsewhere [e.g. 5-7]. In the current work, the possibility of using surface-bonded CFBG sensors to monitor disbonding of a plate-bonded reinforcement has been investigated. This has the potential advantage of using the normal temperature variation between day and night to monitor disbond propagation. In this paper, only the results for the largest temperature change investigated (from room temperature to -30°C) will be presented.

2 Experimental methods

A unidirectional CFRP reinforcement plate (200 mm x 80 mm x 2 mm) was manufactured from T700 carbon fibre unidirectional pre preg tape with a fine glass fibre weft, impregnated with Gurit Prime 20LV resin using the vacuum infusion method. The plate was bonded to a 300 mm long box-section S275 structural steel beam, measuring 100 mm x 100 mm in cross-section and with a wall thickness of 10 mm, using Gurit Spabond 345 room temperature cure structural adhesive, to produce a bondline with a thickness of 2 mm. Two 60 mm uncoated 40% reflectivity CFBG sensors (manufactured by TeraXion), and labelled 1 and 2 in Figure 1, were bonded approximately 26 mm apart on the surface of the CFRP plate, parallel to the length of the plate, using M-Bond AE-10 room temperature cure adhesive. The sensors were placed with the high-wavelength (HW) end of the sensor located approximately 25 mm from the end of the plate. The CFBG sensors had a full width at the half-maximum of the reflected spectrum of 20 nm, and a centre wavelength of 1550 nm. Figure 1 shows a schematic diagram of the plate-bonded steel box-section.

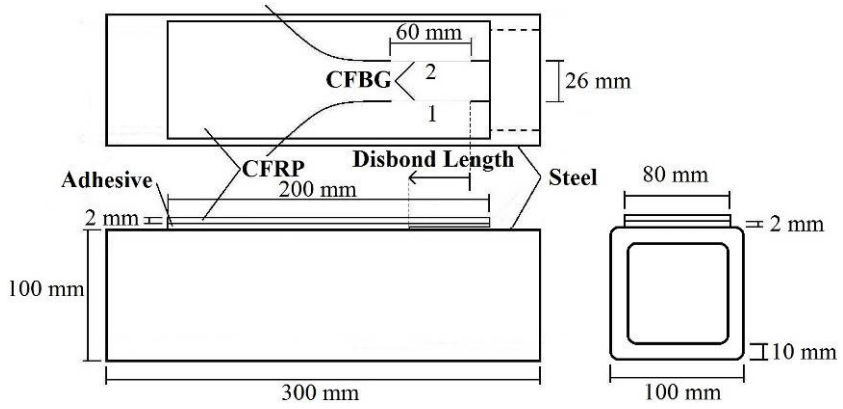

Figure 1. Schematic diagram showing plan (above), side (below) and edge (right) views of a specimen.

It should be noted that all disbond lengths are quoted from the HW end of the CFBG sensor. The dimensions of the steel box-section were chosen so that the flexural stiffness (IE) value of the steel box-section would be very much larger than that of the CFRP reinforcement so as to permit only negligible bending of the plate-bonded steel beam as it was cooled, much as in a bridge structure. The optical fibre sensor was connected to a Smart Fibres W-4 laser interrogator [8] so that the reflected spectra could be captured. To achieve the desired cooling, the plate-bonded box-sections were placed in a Whirlpool ECN 14-1 chest freezer which had

been fitted with an Electrothermal digital MC810B temperature controller which was capable of maintaining temperatures from room temperature down to -30°C in 1°C increments. Disbonds between the CFRP plate and the box-section were introduced using a hacksaw with a blade thickness of 1 mm.

The specimens were placed in the centre of the freezer on a plastic shelf to ensure no direct contact with the interior surface of the freezer. The temperature probe of the thermostat was in direct contact with the steel beam. The leads connecting the CFBG sensor to the laser interrogator, and the temperature probe to the thermostat, passed through a small, well insulated, aperture in the side of the freezer. This allowed the CFBG spectra to be recorded without opening the freezer, and therefore not disturbing the internal temperature. Spectra were recorded for both sensors at room temperature (nominally 21°C) and -30°C. The specimen was then removed from the freezer; a cut was introduced into the adhesive, and then the specimen was replaced in the freezer. The spectra were then recorded at the same temperatures as before. A range of different disbond lengths were investigated.

3 Modelling and prediction of the reflected spectrum of the CFBG sensors

3.1 Appearance of the reflected spectrum

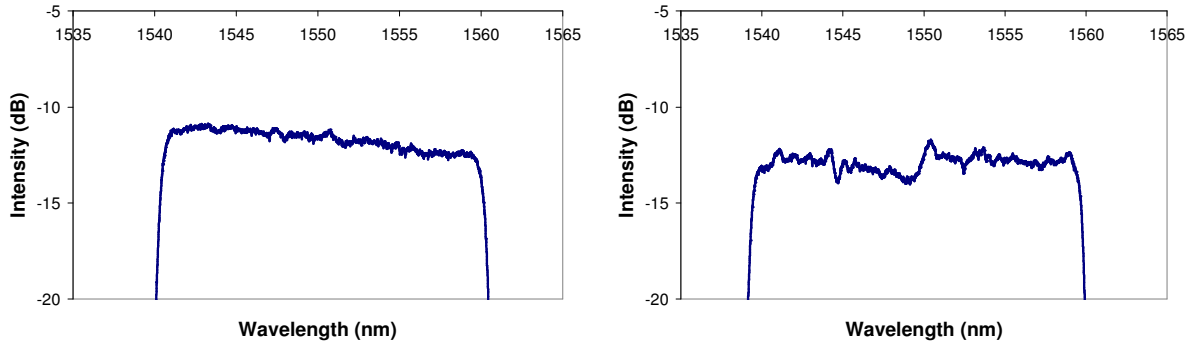

(a) (b)

Figure 2. Experimentally-determined reflected spectrum for a disbond length of 27± 1 mm at (a) room temperature, and (b) at -30°C.

Figures 2(a) and 2(b) shows the reflected spectra for a surface-mounted CFBG sensor with a total disbond length of 52 mm, at room temperature and -30^0C respectively. Since the HW end of the CFBG sensor was located 25 mm from the end of the plate, the disbond extends a distance of about 27 mm with respect to the HW end of the sensor (the disbond extends from the HW end of the sensor towards the LW end of the sensor). The important feature of the spectrum in Figure 2(b) in relation to the disbond is the roughly sinusoidal perturbation which has a trough at a wavelength of approximately 1548 nm and a pronounced peak at approximately 1550 nm. The feature at a wavelength of about 1545 nm is caused by the crimp in the surface longitudinal CFRP tows caused by the occasional glass weft tows.

The physical location of the disbond front could be determined at the edge of the specimen from the location of the hacksaw cut. As indicated above, for the spectrum shown in Figure 2(b), the disbond was approximately 27 mm long with respect to the HW end of the sensor. Within the spectrum, the beginning of the peak-trough pair appears at a wavelength that

corresponds to a distance of about 26 mm from the HW end of the sensor, assuming a linear relationship between distance along the sensor and location within the spectral bandwidth of the sensor (the spectral bandwidth of 20 nm corresponds to physical length of 60 mm). There is therefore good agreement between the physical location of the disbond front and the location of the peak-trough pair in the spectrum. However, to link the peak-trough pair definitively with the location of the disbond front, and to allow the subsequent disbond extension to be measured accurately, it is important to predict the reflected spectrum.

3.2 Prediction of the reflected spectrum

Finite-element (FE) modelling of the specimen was undertaken to predict the axial strain experienced by the surface-bonded optical fibre as a consequence of the disbond and the changing temperature. Predictions of reflected spectra from the CFBG sensors can be made using a commercially available program (OptiGrating, [9]) once the longitudinal strain distribution is known.

The longitudinal strain along the 60 mm sensor length was determined using a 3D FE model. The specimen was modelled for a total disbond length of 52 mm with a range of different mesh sizes, with the finest mesh size (0.0029 mm x 0.0025 mm) at the location of the disbond front. This mesh size was significantly smaller than that required to provide convergence of the results but was required to provide sufficient data resolution as input to OptiGrating. The disbond was modelled as a 1 mm thick cut removed from the adhesive closest to the steel. This resulted in a 1 mm thick layer of adhesive still bonded to the underside of the disbonded CFRP plate. In the modelling results shown here, the FE model assumed that the specimen was manufactured at 20°C and then cooled to -30°C.

The surface longitudinal strain (ε_{11}) along the length of the optical fibres was extracted for a temperature reduction of 50^0C and the results are shown in Figure 3. The vertical line in Figure 3 indicates the position of the disbond front within the model. Note that the line is at a distance of 33 mm from the origin, which is both the location of the LW end of the sensor and adjacent to the still-bonded part of the CFRP plate. At the LW end of the sensor, the initial value of the strain is close to -600 με; this is the strain induced by the cooling of the steel to -30°C, which is the controlling factor regarding the strain in the still-bonded section of the CFRP plate. The longitudinal strain reduces to zero as the disbond front is approached; the precise variation of longitudinal strain is complicated by the high CTE of the steel box-section and the adhesive, and the negligible CTE of the CFRP plate. The strain on the top surface of the CFRP plate becomes tensile in the disbonded region because of the CFRP plate curvature. The curvature occurs because in the disbonded region, there is still a 1 mm thick layer of adhesive that remains bonded to the underside of the plate that causes the plate to bend, putting the surface of the plate into tension. It should be pointed out that, from a practical standpoint, this is an unrealistic aspect of the experiment which has been reproduced in the modelling. In practice, the plate would, of course, be expected to disbond without physical loss of the adhesive. This aspect is addressed in Section 4 below.

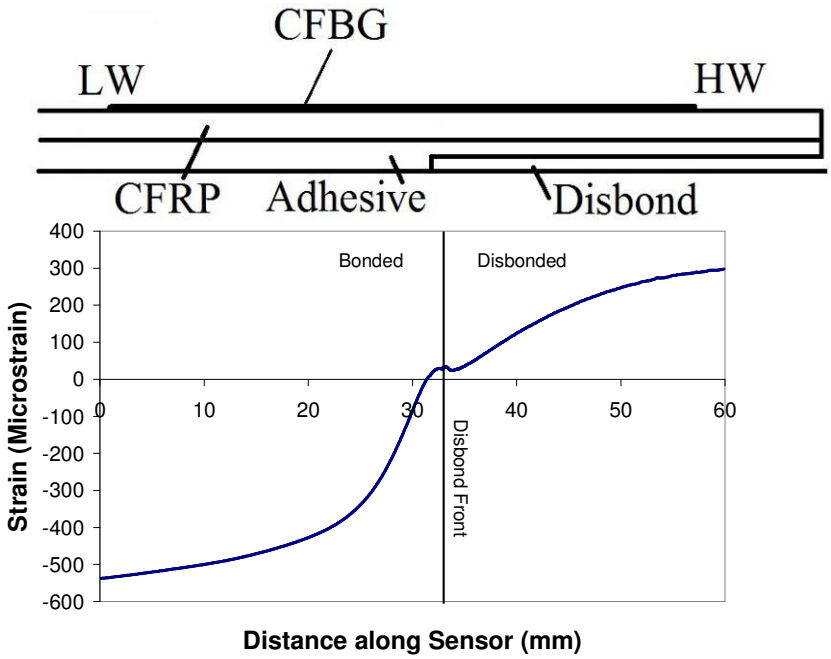

Figure 3. FE strain distribution along the sensor length for a 27 mm disbond at -30°C.

The strain distribution of Figure 3 was then input into OptiGrating. The optical parameters used in the spectrum prediction using OptiGrating were uniform apodization, a Poisson's ratio for the optical fibre of 0.16 and photo-elastic coefficients $p_{11} = 0.113$ and $p_{12} = 0.252$, with an index modulation, Δn, of 0.000219 [12] and a reflectivity of 40%.

Figures 4(a) and (b) show a comparison of a predicted spectrum and the experimentally-recorded reflected spectrum for the same disbond length. Figure 4(a) shows the predicted spectrum for a delamination which is 27 mm in length, using the strain distribution shown in Figure 3. Figure 4(b) shows the experimentally determined reflected spectra from a specimen which included a disbond length of 27mm ± 0.5mm, where the uncertainty arises from the measurement of the disbond length on the specimen edge. It can be seen that there is good agreement between the predicted and experimental reflected spectra. The location of the disbond front within the predicted spectrum in relation to the peak-trough perturbation has been identified by calculating the effect of the strain field on the grating spacing (Λ) and the effective refractive index (n_{eff}) of the sensor and then using the Bragg equation (equation 1) to identify the Bragg wavelength (λ_B) which corresponds to the location of the disbond front.

$$\lambda_B = 2n_{eff}\Lambda \tag{1}$$

It should perhaps be pointed out that, when using a CFBG sensor for the measurement of disbond lengths, the technique is independent of temperature since only relative wavelengths are required. Consequently, uniform changes to the spectrum as a whole, as a result of temperature changes, do not affect such measurements.

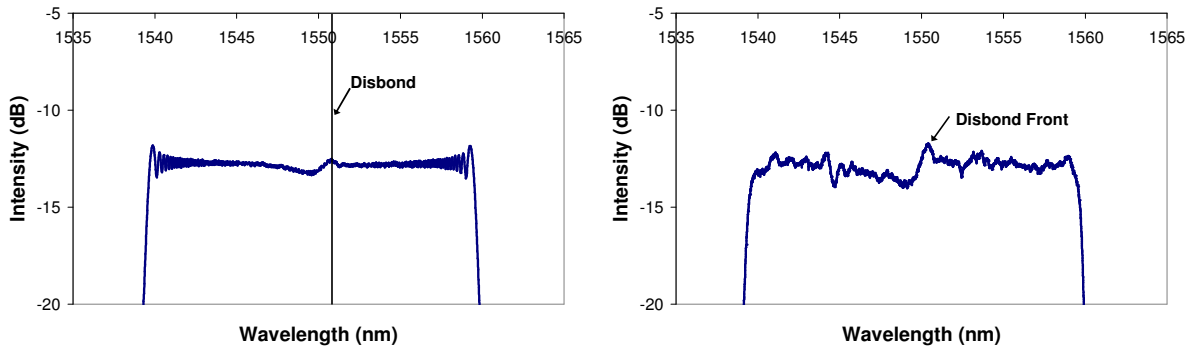

(a) (b)

Figure 4. (a) The predicted spectrum for a disbond length of 27 mm; (b) the experimentally-determined reflected spectrum for a disbond length of 27± 1 mm at -30°C.

4 Experimental monitoring of disbond extension: results and discussion

Typical changes in the reflected spectra for a surface-bonded CFBG sensor for increasing disbond lengths are shown in Figure 5. The sensor was oriented as shown in Figure 3, so that the disbond was extended in length towards the LW end of the sensor.

Figure 5(a) shows the reflected spectra for a specimen which had a 27 mm disbond, and the same specimen with a 37 mm disbond; Figure 5(b) shows the same for disbond lengths of 37 mm and 48 mm. There are two noticeable changes in the reflected spectra as a consequence of disbond growth. The first is that the peak-trough combination, indicative of the location of the disbond, moves to lower wavelengths as the disbond extends in length towards the LW end of the sensor. Figure 6 shows the CFBG measurements of disbond length plotted against the physically measured disbond length for three tests. The results show the disbond lengths measured using the CFBG sensor to be within about 2-3 mm of the physically measured disbond lengths over the entire 60 mm length of the CFBG sensor. The second feature is that the LW-end of the spectra has shifted to higher wavelengths as the disbond progresses. This feature can be understood with reference to Figure 3: as the disbonded length extends, the compressive strain seen by the LW end of the sensor reduces from approximately -540 με to about -500 με for a disbond that is 10 mm longer. Consequently, the compressive strain on these CFBG gratings is relaxed slightly and the LW end of the spectrum moves to higher wavelengths.

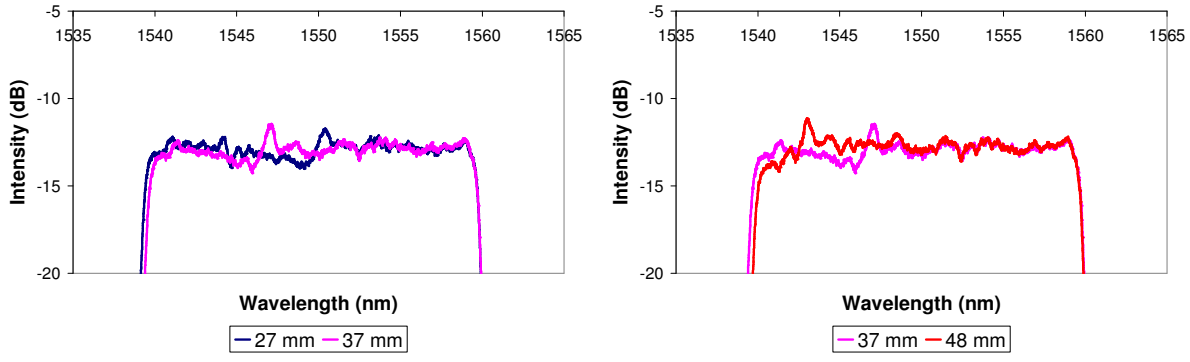

(a) (b)

Figure 5. The reflected spectra from a specimen at -30°C with disbond lengths of (a) 27 mm and 37 mm; (b) 37 mm and 48 mm.

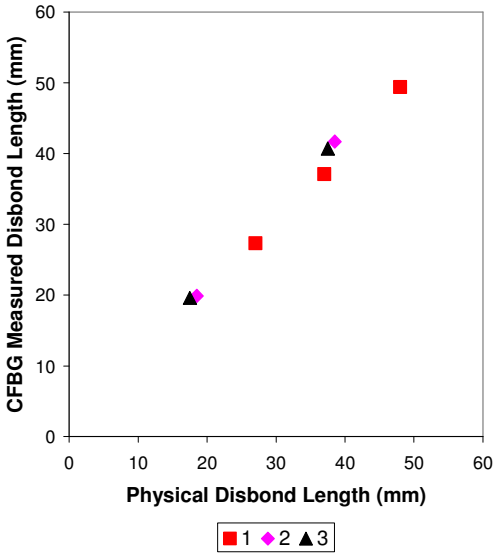

Figure 6. A plot of the disbond lengths determined using the CFBG sensor plotted against the physically measured disbond lengths.

As pointed out above (Section 3.2), the manner of introducing the disbond in these experiments is unrealistic since a hack-saw blade was used to create the disbond, leaving a 1 mm gap between the adhesive still bonded to the CFRP plate and the top of the steel box-section. However, it is possible to use virtual modelling for the more realistic situation, i.e. for a disbond located immediately at the adhesive/steel interface, with no gap. Figure 7(a) shows the strain distribution for the case of a 27 mm disbond, and Figure 7(b) shows the predicted spectrum (for a temperature of -30^0 C). In this case, the resistance to the curvature of the disbonded section of the plate, caused by the contact of the CFRP plate and adhesive with the steel, produces a large compressive strain on the upper surface of the plate, close to the disbond front. This strain distribution produces a reflected spectrum which has a peak in the spectrum corresponding physically to a distance of a few millimetres from the disbond front, on the bonded side of the disbond front (Figure 7(b)), without the associated trough seen in the experimentally-investigated situation (Figure 4(b)). Nonetheless, the location of the disbond can be seen clearly in the predicted spectrum, showing that the CFBG sensor could monitor the disbond front position for this more realistic disbonding case.

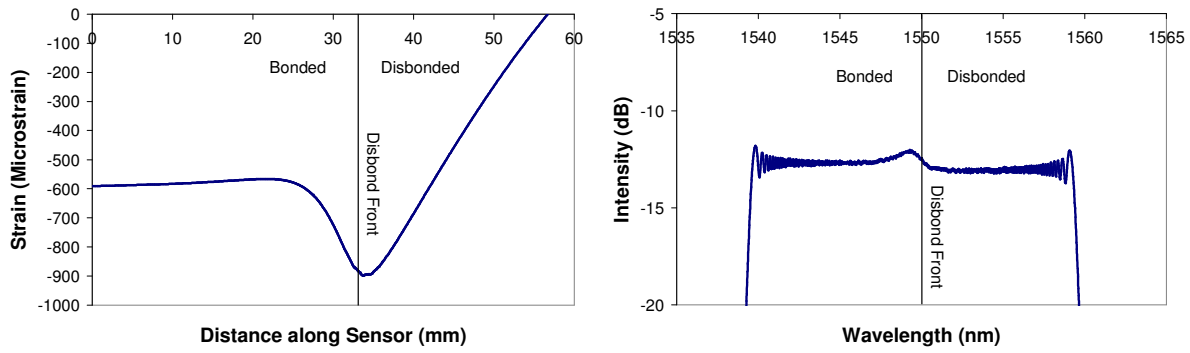

(a) (b)

Figure 7. (a) Longitudinal strain distribution for a disbond of 27 mm at the adhesive/steel interface; (b) predicted reflected spectrum for this case at -30°C.

5 Concluding remarks

Surface-bonded CFBG sensors have been used to monitor the extension of disbonds generated between a CFRP plate-bonded reinforcement and a steel beam using thermally induced strains. The prediction of the reflected spectra was achieved using a combination of finite-element analysis and optical modelling, with good agreement between the predicted spectra and the experimentally measured spectra for a temperature of -30°C. Virtual modelling has also shown that failure of the adhesive bond between the adhesive and the steel box-section (without any gap between the adhesive and the steel) would also produce changes to the spectra which would enable disbond growth to be detected and monitored.

References

[1] Rizzo P., Degala S., Ramanathan K., Harries K.A. Acoustic emission monitoring of CFRP reinforced concrete slabs. *Construction and Building Materials*, **No. 23**, pp. 2016-2026 (2009).

[2] Giurgiutiu V., Harries K.A., Petrou M., Bost J., Quattlebaum J.B. Disbond detection with piezoelectric wafer active sensors in RC structures strengthened with FRP composite overlays. *Earthquake Engineering and Engineering Vibration*, **No. 2**, pp. 1-11 (2003).

[3] Taillade F., Quiertant M., Benzarti K., Aubagnac C. Shearography and pulsed stimulated infrared thermography applied to a non-destructive evaluation of FRP strengthening systems bonded on concrete structures. *Construction and Building Materials*, **No. 25**, pp. 568-574 (2011).

[4] Gebremichael Y.M., Li W., Boyle W.J.O., Meggitt B.T., Grattan K.T.V., McKinley B., Fernando G.F., Kister G., Winter D., Canning L., Luke S. Integration and assessment of fibre Bragg grating sensors in an all-fibre reinforced polymer composite road bridge. *Sensors and Actuators A*, **No. 118**, pp. 78-85 (2005).

[5] Palaniappan J., Ogin S.L., Thorne A.M., Reed G.T., Crocombe A.D., Capell T.F., Tjin S.C., Mohanty L. Disbond growth detection in composite–composite single-lap joints using chirped FBG sensors. *Composites Science and Technology*, **No. 68**, pp. 2410-2417 (2008).

[6] Sanderson A.R., Ogin S.L., Crocombe A.D., Gower M.R.L., Lee R.J. Use of a surface-mounted chirped fibre Bragg grating sensor to monitor delamination growth in a double-cantilever beam test. *Composites Science and Technology, in the press* (2012).

[7] S. Takeda, Y. Okabe, N. Takeda. Monitoring of Delamination Growth in CFRP Laminates using Chirped FBG Sensors. *Journal of Intelligent Material Systems and Structures*, **No. 19**, pp. 437-444 (2008).

[8] Smart Fibres Ltd. W4 Laser Interrogator: User guide and Smartsoft interface instructions.

[9] OptiGrating, Integrated and Fibre Optical Gratings Design Software (version 4.2), Optiwave Corporation, Canada.

[10] BS 5400-3:2000**.** Steel, concrete and composite bridges - Part 3: Code of practice for design of steel bridges (2006).

[11] Peck A.J. *Investigation of FRP stabilization of plastic buckling behaviour of slender steel sections*. MSc Thesis. University of Pittsburgh (2007).

[12] Palaniappan J., Wang H, Ogin S.L., Thorne A., Reed G.T., Tjin S.C., McCartney L.N. Prediction of the reflected spectra from chirped fibre Bragg gratings embedded within cracked cross-ply laminates. *Measurement Science and Technology*, **No. 17**, pp. 1609-1614 (2006).